Vol. 15(4), pp. 213-220, October-December, 2020
DOI: 10.5897/IJPS2020.4924
Article Number: 4306F4C65712
ISSN 1992-1950

http://www.academicjournals.org/IJPS

ACADEMIC JOURNALS
expand your knowledge

International Journal of Physical Sciences

Full Length Research Paper

Coherent perfect absorption in plasmonic planar metasurface

Alamgir Badsha

Department of Physics, Jashore University of Science and Technology, Jashore-7408, Bangladesh.

Received 29 October, 2020; Accepted 3 December, 2020

The coherent perfect absorption (CPA) for a planar resonator of silver has been elaborated here in numerical and analytical approaches. It is investigated numerically in different geometrical shapes and spectral regimes. The CPA mode is observed to be spectrally sensitive to the geometry of the resonator. The scattering matrix method is employed in theoretical analysis. The CPA conditions and output irradiance expressions are extracted. The mode is studied by the relative phase between two counter inputs of the resonator. The appearance of this mode is attributable to the dipole resonance effect. The way light is controlled in the required regime in perfect subwavelength structural geometry is obtained in this study. The nanostructure is functional in optical switching, modulation and terahertz sensor of photonics devices.

Key words: Sensor, modulation, resonator, scattering and finite-difference time-domain (FDTD).

INTRODUCTION

Research on metamaterial is leading people to manipulate light employing 3D or 2D periodical geometry. It paves way for feasible applications of optical devices in visible, near-IR, IR and microwave frequencies. The monolayer of planar, nanoparticle, ring resonator, holes or other shapes of a 2D periodic array of metamaterial is the important development forming artificial interfaces (Edward et al., 2003, Christopher et al., 2005). Bypassing the bulk metamaterial and miniaturization of cavity resonators are the potential contribution of metasurface. In suitable engineering, the reduced dimensional of periodic plasmonic thin film can lead to an unusual propagation direction. Usually these findings are not always available in conventional diffractive optics. Hyperuniform point pattern, resonant metasurface can produce blackbody like absorption (Florian et al., 2019), bandwidth of CPA (Ming et al., 2019) and manipulation of Fresnel coefficients (Jianing et al., 2019) independently. The phase changing effect, transformation of the coordinate of electromagnetic wave is another way of controlling light (Nanfang et al., 2011, Palash et al., 2009) in a 2D array of plasmonic scatterers. Beyond these, the dielectric antenna also shows the resonance effect (Jon et al., 2009). The infinitely periodic structure can be perfectly integrated in optoelectrical devices for phase-shifting surface (Nicolas et al., 2013; Yang, *2008*). Suppressing the resonances, metallic nanodisk can induce the directional scattering in longer wavelength (Staude et al., 2013). In periodic crystal, the slow light mechanism produces nonlinear effects (Zhang et al., 2008, Mork and Nielsen, 2010). Regarding it, the planar plasmonic metamaterial is a suitable candidate for

E-mail: alamgir93_phy@just.edu.bd.

coupling antenna (Na Liu et al., 2010b; Pors et al., 2011). Using the novel plasmonic nanodisk, the localized surface plasmon sensor concepts are to develop experimentally (Na Liu et al., 2010a). Controllable wavelength in silver nanodisk can show transparency and reflectivity as well (Tani et al., 2014). Modulating the amplitude and phase (Nanfang and Federico, 2014; Pors et al., 2014), field enhancement, bio-detection and 3D holographic imaging are the potential applications of metasurface (Smolyaninov et al., 2014; Ni et al., 2013). The lensing characteristics, controlling the polarization densities, terahertz switches, subwavelength resolution are found in these types of optical antenna (Aieta et al., 2013; Holloway et al., 2012; Yu et al., 2013).

Avoiding the complex 3D metamaterials (MMs), the silver resonator was used to study the absorption effect. Numerically, CPA mode is studied by (Lumerical software) finite-difference time-domain (FDTD) method. The absorption is investigated in different spectral and geometrical conditions of the rectangular resonator. It is illuminated normally by two counter input beams from the symmetric structure ($n_0 = n_s = 1$) of unity refractive index of incident (n_0) and substrate (n_s) medium respectively. The development of CPA (Chong et al., 2010; Alamgir et al., 2020; Tae et al., 2016; Ming et al., 2013) mode conditions and output irradiance relations are calculated and satisfied by scattering matrix method. The manipulation of the electromagnetic wave is possible at relative phase variation between the incoming input beams. The analytical expressions are generalized for any planar and nanostructured thin films of symmetric ($n_0 = n_s$) and asymmetric structures ($n_0 \neq n_s$). The appearance of the CPA mode in this nanostructure is attributable to critical coupling and dipole resonance effects. It emphasizes the findings here to be useful in field enhancement, imaging (Smolyaninov et al., 2014; Ni et al., 2013), sensor, modulator, and optical switch (Chong et al., 2010; Alamgir et al., 2020) in photonic devices.

MATERIALS AND METHODS

The plasmonic material of silver (Edward 1998) is used to extract the optical mechanisms by the numerical method of FDTD and the analytical method of scattering matrix. The CPA conditions are extracted elaborately using the scattering matrix method. The propagation direction sets along *x* direction in the normal illumination and is shown in the schematic diagram of Figure 1. The two counter inputs field amplitudes are denoted as E_{in1} and E_{in2} respectively. The two counter outputs field amplitudes are also denoted as E_{out1} and E_{out2} respectively. The reflections and transmissions coefficients are represented (Tae et al., 2016) in terms of scattering matrix as,

$$\begin{bmatrix} E_{out\,1} \\ E_{out\,2} \end{bmatrix} = \begin{bmatrix} r_1 & \tau_2 \\ \tau_1 & r_2 \end{bmatrix} \begin{bmatrix} E_{in\,1} \\ E_{in\,2} \end{bmatrix} \tag{1}$$

In respective incident and substrate medium, the reflection coefficients can be defined with phase and amplitude as $r_1 = |r_1|e^{i\phi_{r1}}$, $r_2 = |r_2|e^{i\phi_{r2}}$; similarly, the transmission coefficients can be denoted with phase and amplitude as $\tau_1 = |\tau_1|e^{i\phi_{\tau 1}}$ and $\tau_2 = |\tau_2|e^{i\phi_{\tau 2}}$. The input irradiances in incident and substrate medium are defined as $I_{in1} = \frac{1}{2} y_0 n_0 |E_{in1}|^2$ and $I_{in2} = \frac{1}{2} y_0 n_s |E_{in2}|^2$ respectively; whereas y_0 is admittance of the vacuum, n_0 and n_s are refractive index of incident and substrate medium respectively.

The transmission coefficients of incident and substrate medium can be expressed in principle of reversibility (Pochi, 2005) as:

$$\tau_1 \sqrt{\frac{n_s}{n_0}} = t_1 = \sqrt{\frac{n_0}{n_s}} \tau_2 = t_2 \tag{2}$$

Normalizing the Equation 1, using Equation 2 yields,

$$\begin{bmatrix} O_1 \\ O_2 \end{bmatrix} = \begin{bmatrix} r_1 & \sqrt{\frac{n_s}{n_0}} t_2 \\ \sqrt{\frac{n_0}{n_s}} t_1 & r_2 \end{bmatrix} \begin{bmatrix} 1 \\ \sqrt{\frac{n_0}{n_s} \frac{I_{in2}}{I_{in1}}} e^{-i\phi_{12}} \end{bmatrix} \tag{3}$$

The normalized input and output amplitude fields are defined as $O_1 = \frac{E_{out1}}{E_{in1}}, O_2 = \frac{E_{out2}}{E_{in1}}$, $E_{in1} = 1$, $\frac{E_{in2}}{E_{in1}} = \frac{|E_{in2}|e^{i\phi_2}}{|E_{in1}|e^{i\phi_1}} = \sqrt{\frac{n_0}{n_s} \frac{I_{in2}}{I_{in1}}} e^{-i\phi_{12}}$.
Here ϕ_{12} is phase difference between two input waves of E_{in1} and E_{in2}.
In the output, when it yields the zero amplitudes such as, $O_1 = O_2 = 0$, then the corresponding reflection and transmission coefficients are produced from Equation 3 as:

$$r_1 = -t_2 e^{-i\phi_{12}} \sqrt{\frac{I_{in2}}{I_{in1}}}, \qquad r_2 = -t_1 e^{i\phi_{12}} \sqrt{\frac{I_{in1}}{I_{in2}}} \tag{4}$$

The product of these coefficients of Equation 4 yields the CPA condition in amplitude relation with Equations 1 and 2 as,

$$r_1 r_2 = t_1 t_2 => \sqrt{R_1 R_2} = T \tag{5}$$

Similarly, the corresponding CPA condition in reflection and transmission phase relationship can be obtained with Equations 1, 2 and 5) as,

$$\phi_t = (\phi_{r1} + \phi_{r2})/2 \tag{6}$$

The output in the incident medium is derived from Equation 3 as,

$$=> I_{out\,1} = \frac{1}{2} y_0 n_0 |O_1|^2$$
$$= \frac{1}{2} y_0 n_0 \left(R_1 + \frac{I_{in2}}{I_{in1}} \; T + 2\sqrt{\frac{I_{in2}}{I_{in1}}} \sqrt{R_1 T} \cos\Delta_1 \right) \tag{7}$$

The forward phase relationship is obtained as $\Delta_1 = \phi_{r_1} - \phi_t - \phi_{12}$

Similarly, the output in the substrate medium is derived from Equation 3 as,

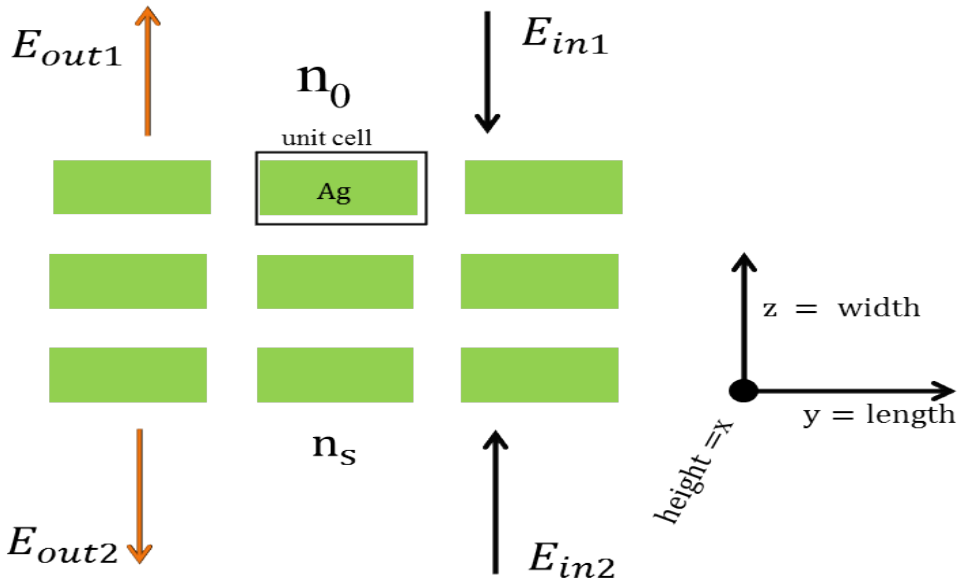

Figure 1. The schematic diagram of plasmonic metasurface.

$$=> I_{out\,2} = \frac{1}{2} y_0 n_s |O_2|^2 = \frac{1}{2} y_0 n_0 \left[T + \frac{I_{in2}}{I_{in1}} \; R_2 + 2 \sqrt{\frac{I_{in2}}{I_{in1}}} \sqrt{R_2 T} \cos\Delta_2 \right] \quad (8)$$

The backward phase relationship can be written as $\Delta_2 = \phi_t - \phi_{r_2} - \phi_{12}$.

The above derived Equations 7 and 8 can be generalized and applicable for any planar and nanostructured thin films to analyze the absorption effect irrespectively in symmetric ($n_0 = n_s$) and asymmetric ($n_0 \neq n_s$) structures.

RESULTS AND DISCUSSION

Analysis of numerical results

The 2D periodic subwavelength spaced in rectangular shape of silver (Edward, 1998) is dealt with here numerically. Simulation results are obtained for symmetric counter input waves in FDTD method. The schematic subwavelength monolayer of metasurface is shown in Figure 2(a).

The plasmonic slab length is studied here for appearance of CPA. In this regard, a relationship between unit cell of the metamaterial and the free space wavelength should be maintained (Smith et al., 2005) for extraction of optical properties. To obtain the optimum dimension of square unit cell for analysis of CPA, the unit cells are studied randomly as discussed in Figure 3(c). Thus a periodic unit cell of $400\,nm$ square lattice of a simulation region is obtained for analysis of optical effect. Periodic boundary condition is used in y and z axes. The perfect matched layer (PML) boundary condition is used in propagation direction of x axis in calculation of CPA spectra as shown in Figure 2(b).

The optimum dimension of the resonator is preconditioned to study the optical properties in this 2D periodic nanostructure. Its thickness is optimally selected as 25 nm. Figure 3(b) shows the perfect width for obtaining the optimum absorption effect. Using these dimensions, optimum length is studied in Figure 2(b) for analysis of optical absorption. The discrete dimensional lengths of the resonator are used. CPA is obtained at 120 nm length and 646 nm wavelength of visible light. No more perfect absorption appeared beyond this resonant length whether it is shorter or longer. The isolated, non-touching unique size slabs and their periodicity develop the cavity resonators at the optimal miniaturization. Thus resonant wavelength is tuned with respect to spatial dimension of the resonators. Beyond the resonant length, modulation takes place at smaller or larger lengths. It implies that the superposition of plane wave front appears as coherent distribution at the same scattering amplitudes of these periodic arrays. The resonant excitation effect of periodic scatterers produces the changing phase and amplitude between backscattered reflection and frontscattered transmission and vice versa leads to the coherent condition of destructive interference (Alamgir et al., 2020). Then the coherent modulation of narrow spectral of Lorentzian line shape of spatial distributions appears. This retardation effect shows the sensitivity of size and shape of the metasurface. Thus the resonators can provide the gradient of spatial distributions. In this way engineering the desired metasurface, optical properties which are not observed in bulk planar thick surface of noble metal, those can be investigated. The dimensional dependency of 2D resonator and the unit cell are investigated in Figure 3 (a, b and c). Keeping the fixed illumination direction, the geometrical shape of the metasurface is studied in

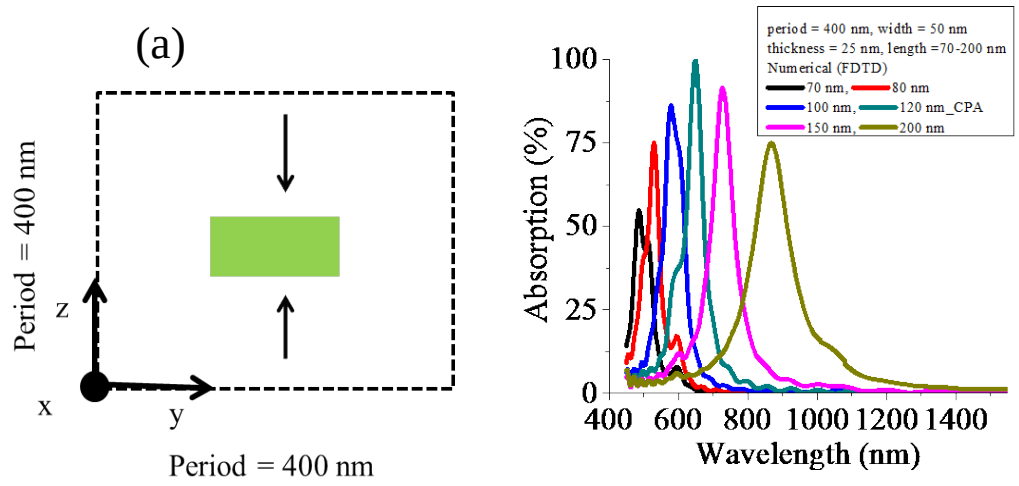

Figure 2. (a) A schematic unit cell of metasurface of silver is drawn for analysis of CPA and (b) Optical Absorption is dependent on the resonator length and spectral range.

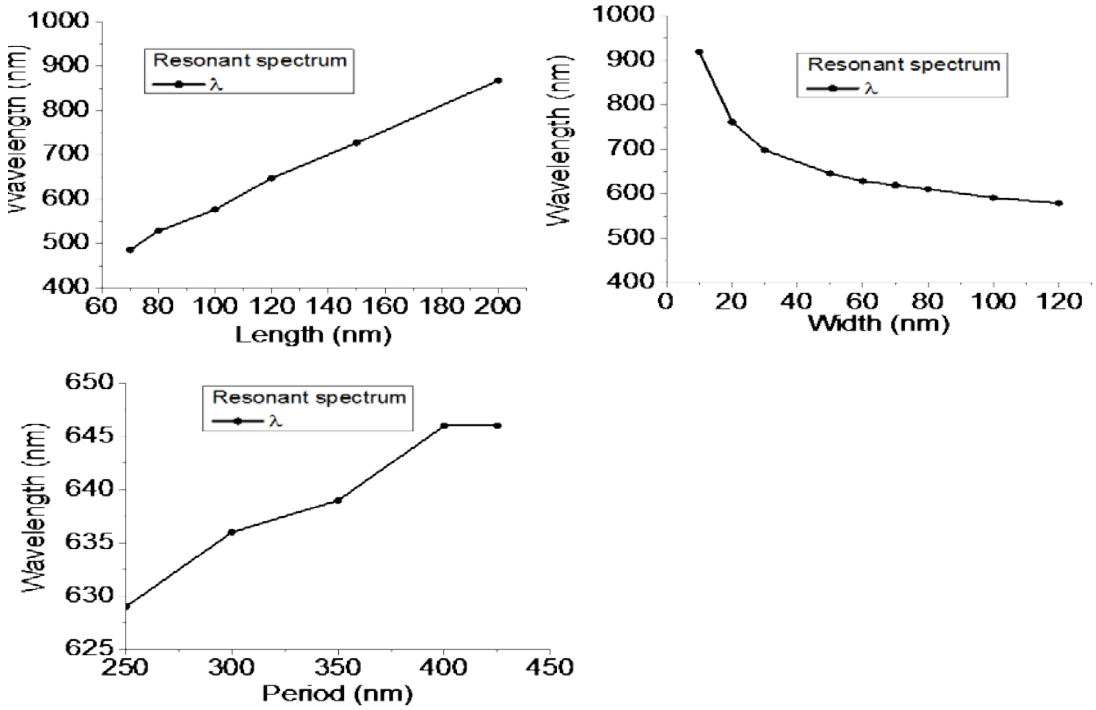

Figure 3. (a, b and c): Investigation of geometrical effect on the resonant absorbing spectral wavelength range with respect to length, width and period of the rectangular scatterers of silver at the same thickness of 25 nm.

different aspects. It represents also the calculated absorbing resonant wavelength with variation of geometrical structures. This study is carried out leaving the dimensions unchanged except the variable one in each case.

It is done due to observation of the spatial phase distribution shifting at the structural effect. Figure 3(a) shows lower length of scatterers, absorption effect appears at visible spectral range. It appears at longer range of near-infrared when the length of the scatterers is extended. Completely opposite phenomena occur for variation of width. Figure 3(b) shows the resonant

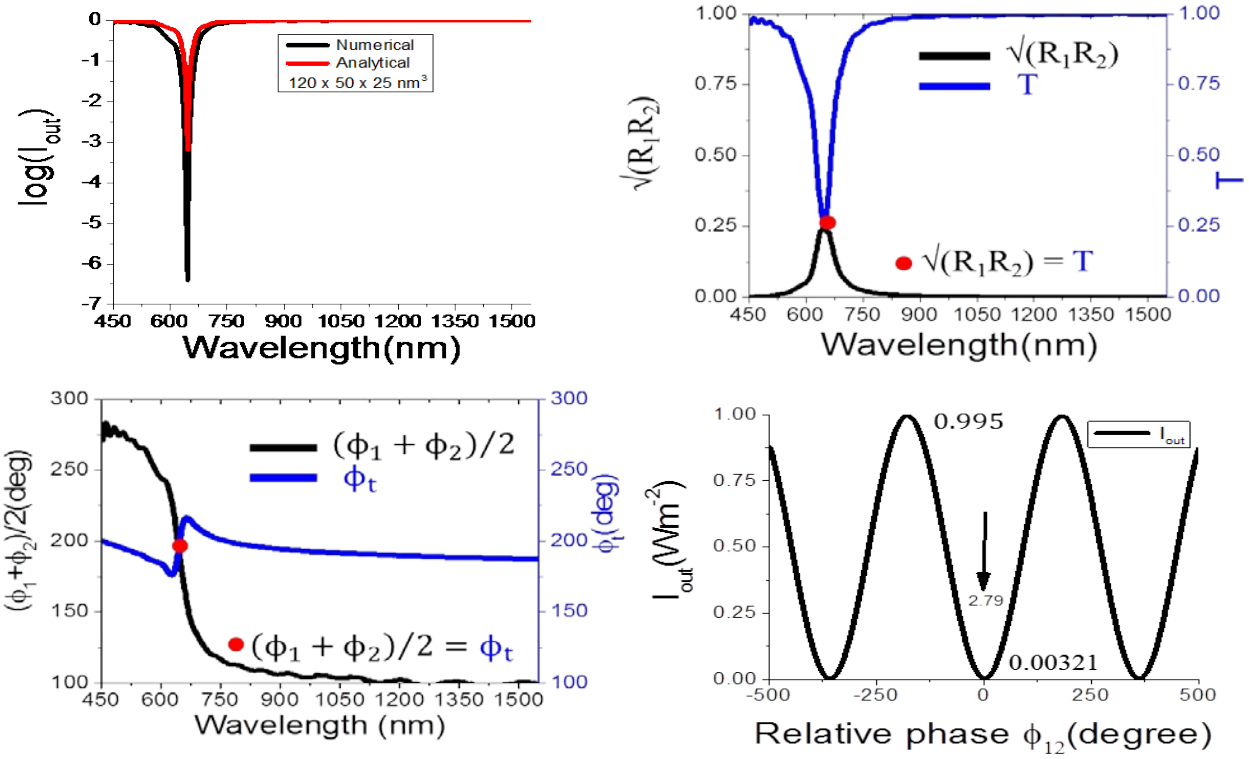

Figure 4. (a) Comparison of numerical (FDTD) and analytical calculations of CPA, (b) The two inputs CPA condition is satisfied at the magnitude of transmittance and reflectance relationship, (c) Similarly the two inputs CPA condition is also satisfied by phase relationship of reflection and transmission coefficients. (d) The normalized irradiance of I_{out} is shown as function of relative phase shift (ϕ_{12}) between two counter inputs.

absorbing regime which is shifting at higher wavelength of near-infrared for lower width of the planar scatterers. The position of resonant wavelength slightly falls as the width size enlarges gradually. Noticeably, at the lower range of width the spectral range falls rapidly. It almost becomes flat at the range of higher width. Figure 3(c) clarifies the enhancement of resonant spectral range is very slower at the enhanced scale of period. The resonance position also stabilizes at higher periodic scale. These effects show the role of subwavelength separation or insulation between the resonators. 99.83% absorption occurs at the extracted CPA dimension of the resonator at the length of 120 nm and width of 50 nm with square unit cell of 400 nm. Beyond these structural and unit cell of dimensions, perfect absorption does not appear. Thus, these geometrical variations extract the sensitivity of the length and width in analysis of 2D periodic nanostructure. Through these analyses, it is clear that resonant mode may appear at time-reversal symmetry excitation (Chong et al., 2010; Alamgir et al., 2020) in visible to near-infrared regions in the silver metasurface depending on the dimensional parameters. Considering these resonant spectral position sensitivity, it is convenient to select the perfect design and structure in symmetric periodic metasurface. It convinces the role of controllable smart surface (Edward et al., 2003, Christopher et al., 2005) at visible to near-infrared spectral range.

Analysis of analytical results

Using the CPA dimension of the resonator, the logarithmic values of normalized output irradiances are presented in Figure 4(a) as function of wavelength. The numerical calculation which is obtained by FDTD (black line) and the analytically calculated (red line) spectra are similar in pattern. The analytical spectrum is calculated using the Equation 7. The output irradiances at CPA wavelength are shown nearly zero. Beyond the phase and irradiance matching, the scattered irradiance enhances and reduces the absorption gradually as incoherent incoming input waves increasing. This occurs as the enhancement of constructive interference. Two alternative methods are applied here to verify the CPA conditions. One is matching relation of reflection and transmission coefficients and another is corresponding phase matching relation. The two CPA conditions are drawn in Figure 4(b, c). Figure 4(b) represents graphically at variable wavelength, the product of magnitudes of

reflectance in each medium (black curve) and transmittance (blue curve) $\left(T = \sqrt{R_1 R_2}\right)$. Each of these spectra is distinguishable by means of their spectral characteristics. These spectra show the single intersection coordinate which is corresponding to the CPA wavelength.

They carry the same magnitude and hence the coupling condition satisfies at the minimum value of transmittance and the maximum or peak value of reflectance. This resonance coupling produces the destructive interference effect as CPA at coherent wavelength of phase matching condition. Beyond the resonance wavelength constructive interference enhances as the transmittance spectrum shows which is a single dip. The opposite phenomena occur in case of spectrum of reflectance especially around the resonance wavelength. Figure 4 (c) shows the phase relationship of reflection coefficients and transmission coefficient $(\phi_t = (\phi_{r1} + \phi_{r2})/2)$. The total reflection phase of incident and substrate medium slightly falls as wavelength increases which is noticeable in the whole range of the spectrum. Expectedly, at the CPA spectral position, opposite phenomenon occurs in case of transmission phase. The intersection point of both phases is located corresponding to the CPA resonance spectrum. In these ways the phase matching conditions are satisfied separately.

The output irradiances are also plotted in Figure 4(d) as function of relative input phase ϕ_{12} in CPA wavelength. It shows that beyond the relative phase 2.79 (in degree) of CPA mode, irradiances increase uniformly as the effect of constructive interference between scattered amplitudes in the output medium. The sensitivity of relative phase between two inputs is obvious. The maximum and minimum output irradiances are calculated as 0.995 and 0.00321 respectively in corresponding peaks and dips. These characteristics may help to select the required design accordingly as the controllable miniaturized surface (Edward et al., 2003; Christopher et al., 2005). On the other hand, these are the indications of probable applications of optical switching (Chong et al., 2010, Alamgir et al., 2020) or modulator in the integrated connectors (Michal, 2005) of this plasmonic metasurface.

Analysis of CPA mode characteristic

Now the mechanism of mode can be extracted. It can be analyzed by temporal coupled mode theory (TCMT) (Fan et al., 2003) as multiport illumination system. The calculated absorption in TCMT and FDTD are presented comparatively in Figure 5(a). The plasma resonance absorption (PRA) as 50% is calculated by the single input illumination. It is attributable to the inherent absorbing effect of intrinsic damping (g_i) of the plasmonic material. The CPA modes are calculated by both methods in multiport illumination system. TCMT is corresponding to the critical coupling condition (CC) (Ming et al., 2013; Alamgir et al., 2014). The condition of CC is related to radiative damping (g_r) which must be equal to the intrinsic damping (g_i). It is obtained as $g_r = g_i = 5.832\ \mathrm{Hz}$. Thus developed CPA mode is here related to the CC. The PRA and CPA both modes produce well matching with the numerical calculations. There is little mismatching scattering effect between these calculations of two methods at shorter spectrum. These are observable far away in the regime of less than resonant spectrum of 646 nm.

Another way can be applicable here to extract the development mechanism of this mode. It is done by observing the electric field profile in the resonator. The incident light is propagated in normal direction along x axis to the resonator which is shown in Figure 5(b). The electric field profile is shown in different color as variation of dissipated energy. The redistribution effect of scattering is consistent in this field profile. It is understandable the way of dissipation and scattering occurs by the CPA mode at resonance condition. The localized surface plasmon (LSP) can be attributable to this. It is related to the metallic non-radiative optical phenomenon of condensing the incoming plane waves in the metasurface. Herein each corner polarized dipoles are developed which are the satisfaction of resonance condition. The electric field irradiance is intensively high; it is indicated as red color near the each dipole. It is inverse square proportional to the distance from the center of the dipole. That is why this magnitude gradually decreases and is indicated by green color as it is away from the corner of the dipole resonance locations. As the profile irradiance color bar shows, some amount of energy is also confined inside the rectangular resonator due to the inherent plasmonic absorption effect. These optical phenomena are ascribable for the development of CPA in this article.

These characteristics of subwavelength separated optical scatterers are encouraging in implementation as optical antennas, resonators and sensing devices. The wavefront shaping technique is applicable also in integrated optical device of modulation functionality in different frequency regimes according to size and shape of the scatterers as the controllable surface (Edward et al., 2003; Christopher et al., 2005).

Conclusion

Instead of complex structured 3D MMs, the numerical and analytical approaches are employed in this 2D plasmonic resonator to extract the CPA. The absorption effect is analyzed in different spectral aspects and geometrical shapes of the metasurface. The extracted CPA conditions and output irradiance are satisfied analytically. The output irradiances are obtained as peaks (0.995) and dips (0.00321) by controlling the relative phase between two counter inputs, which are the important finding for modulation and switching devices.

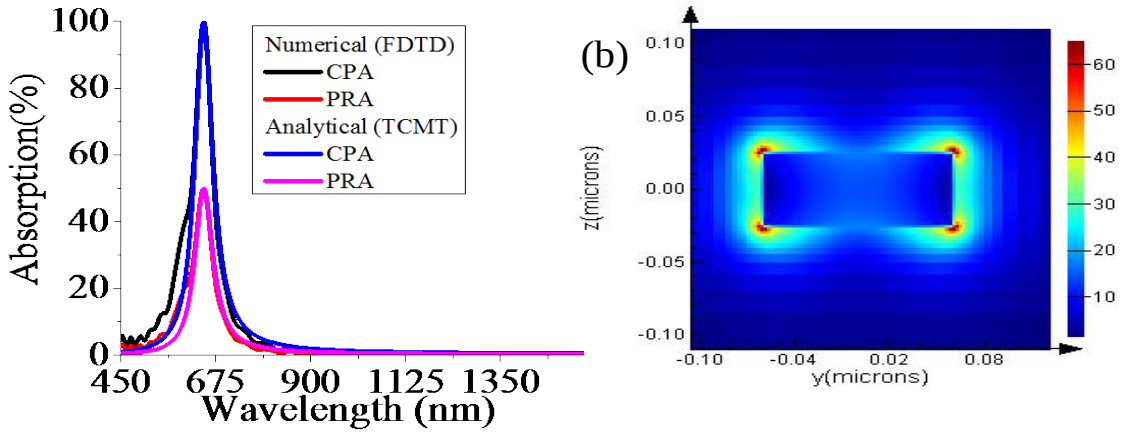

Figure 5. (a) The CPA mode is extracted by temporal coupled mode theory (TCMT) and (b) The development mechanism of CPA mode is visualized by electric field $|E_x|^2$ irradiance ($Js^{-1}m^{-2}$) profile in symmetric structure ($n_0 = n_s = 1$) of counter beams propagated along x-direction at resonance wavelength of 646 nm for the dimension of $120 \times 50 \times 25\ nm^3$ of the scatterers.

The theoretical derivations are generalized for any planer and nanostructured thin films. The critical coupling and dipole resonance effects may be ascribed to the appearance of this absorption mode. Thus this resonator can provide the spatial amplitude and phase shifting distributions. The way light is controlled in the required regime in perfect subwavelength structural geometry is obtained in this work. It can be applied as terahertz sensor, modulator and optical switching in photonic devices.

CONFLICT OF INTERESTS

There is no conflict of interest.

ACKNOWLEDGEMENT

This work is supported by the research project of Jashore University of Science and Technology, Bangladesh.

REFERENCES

Aieta F, Genevet P, Kats M, Capasso F (2013). Aberrations of flat lenses and aplanatic metasurfaces. Optics Express 21(25):31530-31539. https://doi.org/10.1364/OE.21.031530

Alamgir B Md., Mohammad AR, Humaun K Md., Mehade H Md. (2020). Coherent perfect absorption in epsilon-near-zero ITO thin film in near infrared. Optica Pura Y Aplicada 53(1):1-12. http://dx.doi.org/10.7149/OPA.53.1.51031

Alamgir Badsha Md., Humaun Kabir Md., Mohammad Abdur Rashid (2020). Coherent perfect absorption in unpatterned thin films of intrinsic semiconductor. Journal of Optics 49(3):342-350. https://doi.org/10.1007/s12596-020-00624-4

Alamgir B Md., Young Chul Jun, Chang Kwon Hwangbo (2014). Admittance matching analysis of perfect absorption in unpatterned thin films. Optics Communications 332:206-213. https://doi.org/10.1016/j.optcom.2014.07.004

Christopher LH, Mohamed A.M, Edward F. Kuester, Andrew Dienstfrey (2005). Reflection and transmission properties of a metafilm: with an application to a controllable surface composed of resonant particles. IEEE transaction on electromagnetic. Compatibility 47(4):853-865. https://doi.org/10.1109/TEMC.2005.853719

Chong YD, Li G, Hui C, Stone AD (2010). Coherent perfect absorbers: time-reversed lasers. PRL 105(5):053901. https://doi.org/10.1103/PhysRevLett.105.053901

Edward DP (1998). Handbook of Optical Constants of Solid II. Academic Press, INC.

Edward F. Kuester, Mohamed A. Mohamed, Melinda Piket-May and Christopher L. Holloway (2003). Averaged transition conditions for electromagnetic fields at a metafilm. IEEE Transaction on Antennas and Propagation 51(10):2641-2651. https://doi.org/10.1109/TAP.2003.817560

Florian Bigoourdan, Romain Pierrat, Remi Carminati (2019). Enhanced absorption of waves in stealth hyperuniform disordered media. Optics Express 27(6):8666-8682. https://doi.org/10.1364/OE.27.008666

Fan S, Suh W, Joannopoulos JD (2003). Temporal coupled-mode theory for the Fano resonance in optical resonators. Journal of Optical Society of America A 20(3):569-572. https://doi.org/10.1364/JOSAA.20.000569

Holloway CL, Kuester EF, Gordon JA, Hara JO, Booth J, Smith DR (2012). An overview of the theory and applications of metasurfaces: the two-dimensional equivalents of metamaterials. IEEE Antenna and Propagation Magazine 54(2):10-35. https://doi.org/10.1109/MAP.2012.6230714

Jianing Yang, Xiaoyu Wu, Jiakun Song, Cheng Huang, Yijia Huang, Xiangang Luo (2019). Cascaded metasurface for simultaneous control of transmission and reflection. Optics Express 27(6):9061-9070. https://doi.org/10.1364/OE.27.009061

Jon A. Schuller, Mark L. Brongersma (2009). General properties of dielectric optical antennas. Optics Express 17(26):24084-24095. https://doi.org/10.1364/OE.17.024084

Mork J, Nielsen TR (2010). On the use of slow light for enhancing waveguide properties. Optics Letters 35(17):2834-2836. https://doi.org/10.1364/OL.35.002834

Michal L (2005). Guiding, modulating, and emitting light on silicon—challenges and opportunities. Journal of Lightwave Technology 23(12):4222-4238. https://www.osapublishing.org/jlt/abstract.cfm?URI=jlt-23-12-4222

Ming K, Fu Liu, Teng-Fei Li, Qing-Hua G, Jensen Li, Jing C (2013). Polarization-independent coherent perfect absorption by a dipole-like metasurface. Optics Letters 38(16):3086-3088. https://doi.org/10.1364/OL.38.003086

Ming K, Ming Li, Jing C (2019). Bandwidth bounds of coherent perfect absorber in resonant metasurfaces. Optics Express 27(6):9004-9012. https://doi.org/10.1364/OE.27.009004

Na Liu, Martin Mesch, Thomas Weiss, Mario Hentschel, Harald Giessen (2010a). Infrared perfect absorber and its application as plasmonic sensor. Nano Letters 10(7):2342-2348. https://doi.org/10.1021/nl9041033.

Na Liu T, Weiss TM, Mesch ML, Langguth LU, Eigenthaler UM, Hirscher MC, Sonnichsen, H, Giessen H (2010b). Planar metamaterial analogue of electromagnetically induced transparency for plasmonic sensing. Nano Letters 10(4):1103-1107. https://doi.org/10.1021/nl902621d

Nanfang Yu, Federico C (2014). Flat optics with designer metasurfaces. Nature Materials 13: 139-150. https://doi.org/10.1038/nmat3839

Nanfang Yu, Patrice G, Mikhail AK, Francesco A, Jean-Philippe T, Federico C, Zeno G (2011). Light propagation with phase discontinuities: generalized laws of reflection and refraction. Science, 334(6054): 333-337. DOI: 10.1126/science.1210713

Nicolas G, Aldo P, Derek AM (2013). Research and development on phase-shifting surfaces (PSSs). IEEE Antennas and Propagation Magazine 55(2):30-48. https://doi.org/10.1109/MAP.2013.6529314

Ni X, Kildishev AV, Shalaev V (2013). Metasurface holograms for visible light. Nature Communications 4:2807. https://doi.org/10.1038/ncomms3807

Pochi Y (2005). Optical Waves in Lalyered Media. Chapter 3, A John Wiley and Sons Inc. Publication, New Jersey, United States of America.

Pors A, Neilsen MG, Roberts AS, Bozhevolnyi SI (2014). Gap plasmon-based metasurfaces: from amplitude to phase control of reflected light. 8th International Congress on Advanced Electromagnetic Materials in Microwaves and Optics 400-402. https://doi.org/10.1109/MetaMaterials.2014.6948574

Pors A, Nielsen MG, Velle GD, Willatzen M, Albrektsen O, Bozhevolnyi SI (2011). Plasmonic metamaterial wave retarders in reflection by orthogonally oriented detuned electrical Dipoles. Optics Letters 36(9):1626-1628. https://doi.org/10.1364/OL.36.001626

Palash B, Bradley D, Lukas N (2009). Optical antennas. Advance in Optics and Photonics 1(3):438-483. https://doi.org/10.1364/AOP.1.000438

Smolyaninov A, Pang L, Freeman L, Abashin M and Fainman Y (2014). Broadband metacoaxial nanoantenna for metasurfac and sensing applications. Optics Express 22(19):22786-22793. https://doi.org/10.1364/OE.22.022786

Smith DR, Vier DC, Koschny Th, Soukoulis CM (2005). Electromagnetic parameter retrieval from inhomogeneous metamaterials. Physical Review E 71(3):036617. https://doi.org/10.1103/PhysRevE.71.036617

Staude I, Miroshnichenko AE, Decker M, Fofang NT, Liu S, Gonzales E, Dominguez J, Luk TS, Neshev DN, Brener I, Kivshar Y (2013). Tailoring directional scattering through magnetic and electric resonances in subwavelength silicon nanodisks. American Chemical Society Nano 7(9):7824-7832. https://doi.org/10.1021/nn402736f

Tani T, Hakuta S, Kiyot N, Naya M (2014). Transparent near-infrared reflector metasurface with randomly dispersed silver nanodisks. Optics Express 22(8):9262-9270. https://doi.org/10.1364/OE.22.009262

Tae Young Kim, Md. Alamgir Badsha, Junho Yoon, Seon Young Lee, Young Chul Jun, Chang Kwon Hwangbo (2016). General strategy for broadband coherent perfect absorption and multi-wavelength all-optical switching based on epsilon-near-zero multilayer films. Scientific Rep. 6:22941. https://doi.org/10.1038/srep22941

Yu N, Genevet P, Aieta F, Kats MA, Blanchard R, Aoust G, Tetienne JP, Gaburro Z, Capasso F (2013). Flat optics: controlling wavefronts with optical antenna metasurfaces. IEEE Journal of Selected Topics in Quantum Electronics 19(3):4700423. https://doi.org/10.1109/JSTQE.2013.2241399

Yang Y (2008). Analytic solution of free space optical beam steering using Risley prisms. Journal of Lightwave Technology 26(21):3576-3583. https://doi.org/10.1109/JLT.2008.917323

Zhang S, Genov DA, Wang Y, Liu M, Zhang X (2008). Plasmon-induced transparency in metamaterials. PRL 101(4):047401. https://doi.org/10.1103/PhysRevLett.101.047401